aSupplementary Information
for
Fabrication of Potential Environmentally Friendly 3D Printing Filament Biocomposites Based on Poly(lactic acid) and Cellulose Fibers from Agricultural Waste

Nguyen Chi Thanh,[a*] Pham Duc Thinh,[a] Bui Phuong Dong,[a] Tran Hai Cat ,[a] and Nguyen Thanh Huy [b,c]

[a] Faculty of Applied Sciences, Ho Chi Minh City University of Technology and Engineering, 01 Vo Van Ngan Street, Thu Duc Ward, Ho Chi Minh City, Vietnam.

[b] Department of Polymer Materials, Faculty of Materials Technology, Ho Chi Minh City University of Technology (HCMUT), 268 Ly Thuong Kiet Street, District 10, Ho Chi Minh City, Vietnam.

[c] Vietnam National University Ho Chi Minh City, Thu Duc Ward, Ho Chi Minh City, Vietnam.

Email: Nguyen Chi Thanh - thanhnc@hcmute.edu.vn

* Corresponding author

Table S1. One-way ANOVA table of crystallinity index of the CC and CMF-TL samples.

Source	Sum of Squares	Df	Mean Square	F-Ratio	P-Value
Between groups	0.371	2	0.186	0.217	0.811
Within groups	5.127	6	0.855		
Total	5.498	8			

Changes in the raw material-to-chemical solution ratios do not significantly influence the crystallinity index of the CMF.

Table S2. One-way ANOVA table of crystallinity index of the CC and CMF-T samples.

Source	Sum of Squares	Df	Mean Square	F-Ratio	P-Value
Between groups	27.870	2	13.935	14.868	0.00473
Within groups	5.623	6	0.937		
Total	33.493	8			

Changes in the reaction temperatures significantly influence the crystallinity index of the CMF.

Table S3. One-way ANOVA table of crystallinity index of the CC and CMF-t samples.

Source	Sum of Squares	Df	Mean Square	F-Ratio	P-Value
Between groups	107.996	2	53.998	63.326	7.136×10^{-5}
Within groups	4.673	6	0.779		
Total	112.669	8			

Changes in the reaction time significantly influence the crystallinity index of the CMF.

Table S4. Mechanical properties of neat PLA and PLA biocomposites reinforced with CMF and RBO-modified CMF at different contents.

Sample	Tensile Strength (MPa)	Elongation at break (%)	Young's Modulus (MPa)
PLA	40.27 ± 3.46	1.73 ± 0.16	22.38 ± 3.11
PLA/CMF1	20.51 ± 3.75	1.52 ± 0.06	15.44 ± 3.01
PLA/CMF5	25.20 ± 0.74	1.27 ± 0.20	21.47 ± 3.64
PLA/CMF10	17.60 ± 1.83	0.99 ± 0.04	18.17 ± 2.73
PLA/RBO1	41.23 ± 7.64	1.82 ± 0.28	24.38 ± 3.48
PLA/RBO5	19.79 ± 1.10	1.44 ± 0.07	16.75 ± 2.43
PLA/RBO10	14.13 ± 1.77	1.12 ± 0.16	15.95 ± 2.28

Table S5. The parameters of the 3D printing process.

Parameter	**Value**
Nozzle diameter (mm)	0.4
Printing temperature (°C)	190
Bed temperature (°C)	60
Printing speed (mm/s)	50
Infill density (%)	15
Layer hight (mm)	0.2
Printing flow (%)	100

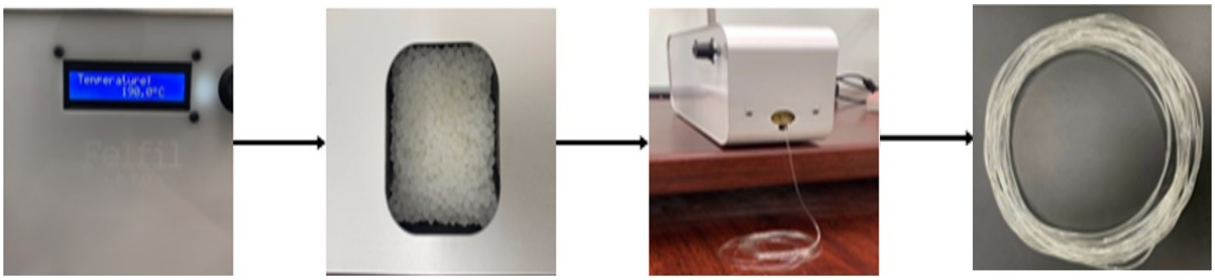

Fig S1. Fabrication of PLA/CMF Filament

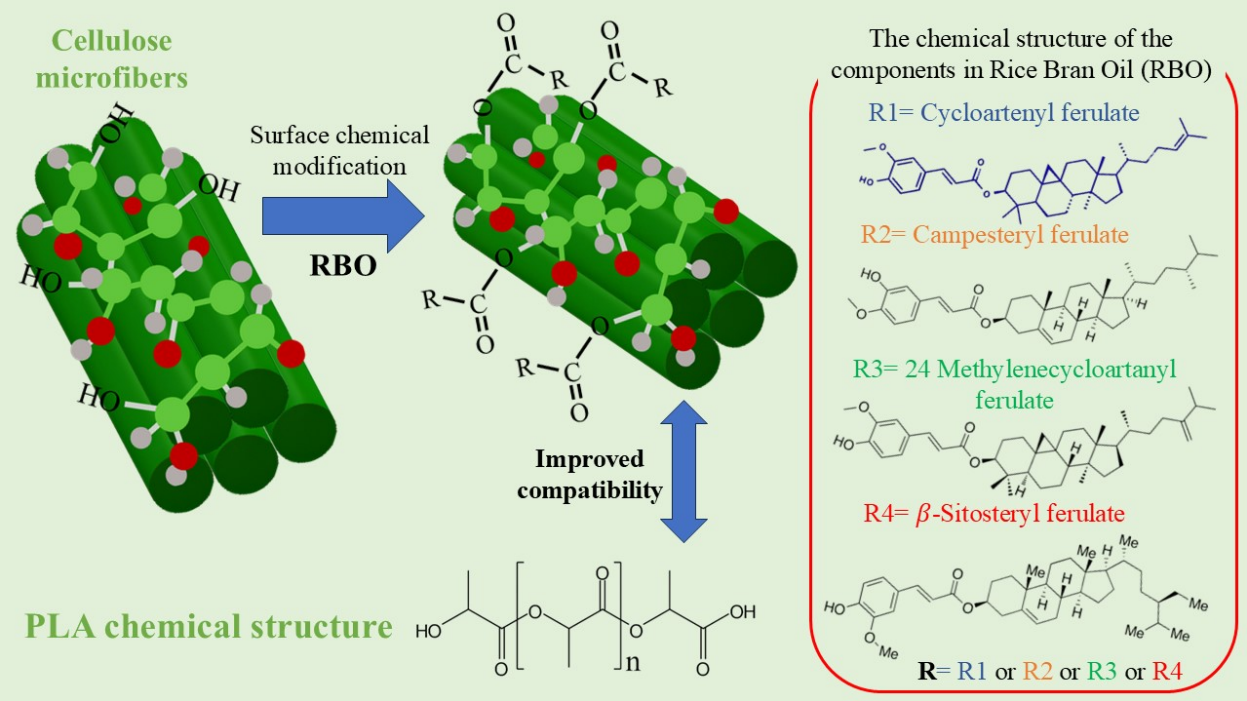

Fig S2. Description of the reaction mechanism between the extracted cellulose fibers and rice bran oil (RBO)

Rheological properties

The rheological measurements were conducted exclusively on the RBO-modified composites to systematically investigate the influence of fiber content on melt flow behavior and processability. Figure S3 presented the viscosity curves of neat PLA and PLA/CMF biocomposites measured at 170 °C. The results clearly showed that melt viscosity increased with increasing CMF content, particularly in the low shear rate region. This behavior was attributed to the large specific surface area of cellulose fibers and their tendency to form a percolated network structure, which restricted polymer chain mobility.[1,2] At higher shear rates, pronounced shear-thinning behavior was observed, as the cellulose fibers tended to align along the flow direction, thereby reducing fiber–fiber and fiber–matrix interactions.[3] For composites containing 5 and 10 wt% CMF, viscosity reduction with increasing shear rate was still evident; however, the trend became less uniform compared to composites with lower fiber loadings. This phenomenon was explained by non-uniform fiber dispersion and the formation of fiber agglomerates, leading to uneven breakdown and restructuring of the fiber network under shear deformation. Notably, the PLA/CMF composite containing 1 wt% cellulose fiber exhibited an optimal balance between melt strength and flowability, which was favorable for filament stability during extrusion and for interlayer adhesion during 3D printing.

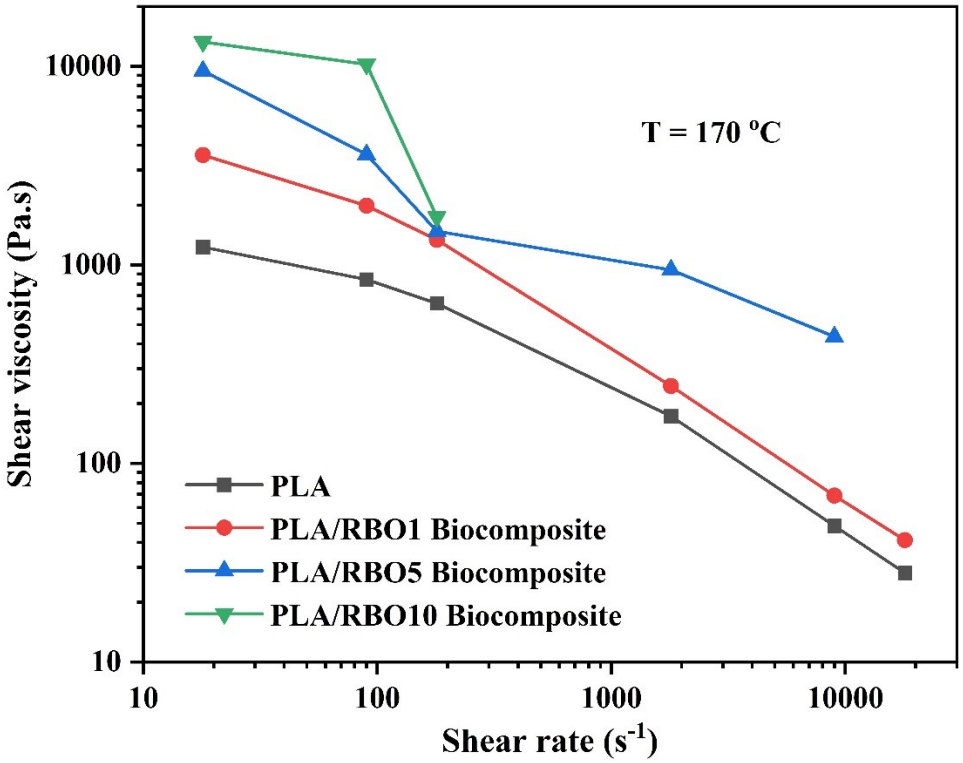

Fig. S3. Flow curves of PLA and biocomposites with different fiber loadings.

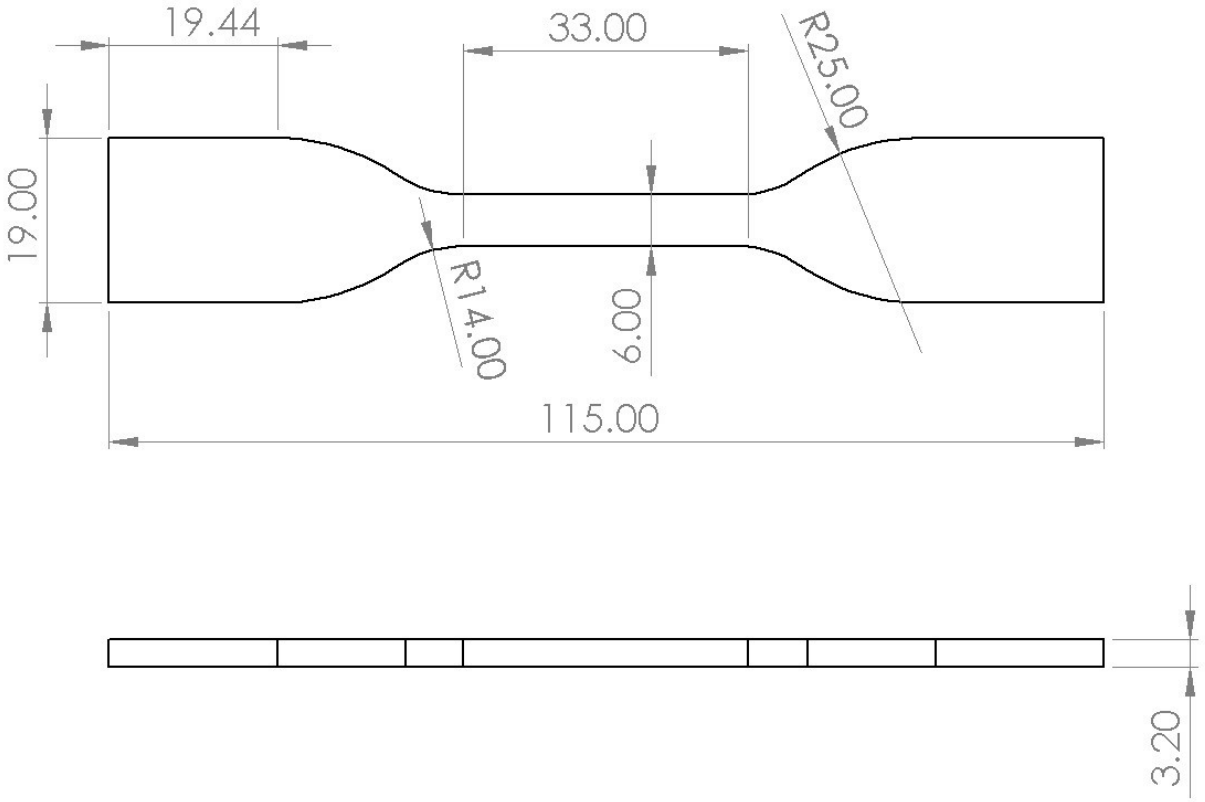

Fig S4. Dimensional specifications of ASTM D638 Type IV tensile specimens.

Mechanical properties of 3D-printed samples

Figure S5 presented the stress–strain curves of 3D-printed neat PLA and PLA/RBO composites containing 1 wt% rice bran oil (RBO)–modified cellulose. The 3D-printed PLA/RBO samples exhibited a tensile strength and elongation at break of 31.61 ± 0.74 MPa and 2.15 ± 0.12%, respectively, which were higher than those of neat 3D-printed PLA (28.62 ± 1.05 MPa and 2.05 ± 0.17%). These results were consistent with the mechanical properties observed for the composite samples prior to printing, indicating that the reinforcing effect of the modified cellulose was stably maintained throughout the filament extrusion and 3D printing processes. The observed improvement was attributed to enhanced compatibility between the modified cellulose and the PLA matrix, which promoted more efficient stress transfer and reduced stress concentration sites. In addition, the modified cellulose contributed to stabilizing the melt flow behavior and improving interlayer bonding during printing, thereby enhancing the overall mechanical performance of the 3D-printed parts.

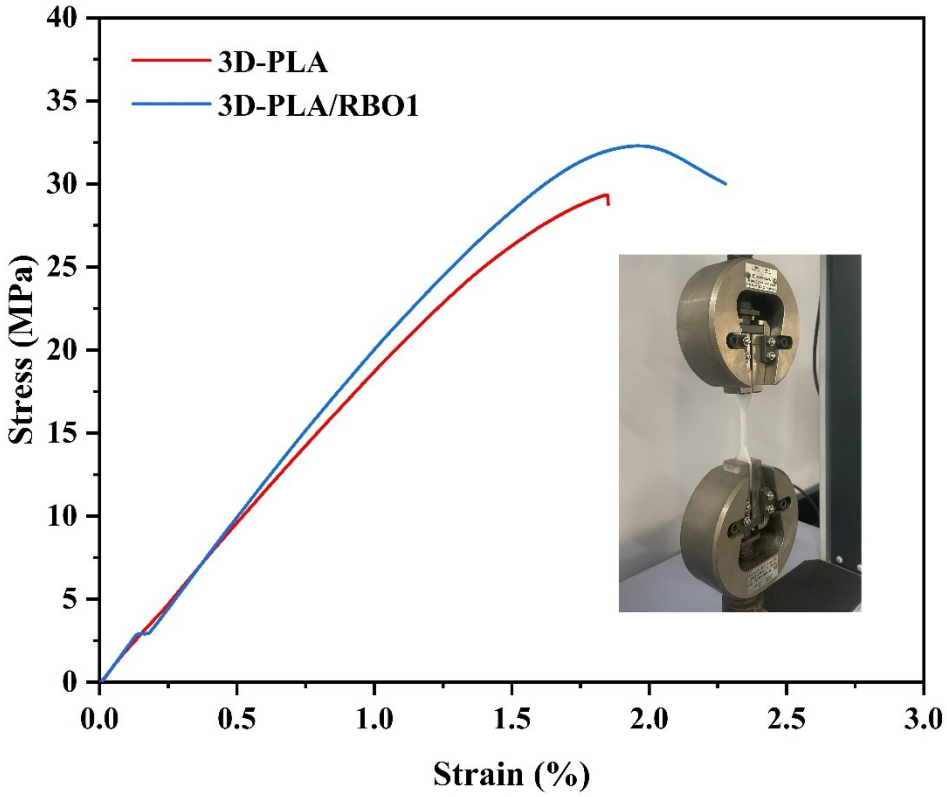

Fig S5. Stress–strain curves of the 3D-printed samples.

References

1. M. Lecoublet, M. Ragoubi, N. Leblanc and A. Koubaa, Industrial Crops and Products, 2024, 221, 119332.
2. S. Y. Cho, H. H. Park, Y. S. Yun and H.-J. Jin, Macromolecular Research, 2013, 21, 529-533.
3. W. Ding, T. Kuboki, A. Wong, C. B. Park and M. Sain, RSC advances, 2015, 5, 91544-91557.